



Using 4-km WRF CONUS simulations to assess impacts of the surface coupling strength on regional climate simulation

Liang Chen^{1,2} · Yanping Li² · Fei Chen³ · Michael Barlage³ · Zhe Zhang² · Zhenhua Li²

Received: 1 January 2018 / Accepted: 7 August 2019 / Published online: 21 August 2019
© Springer-Verlag GmbH Germany, part of Springer Nature 2019

Abstract

Uncertainties in representing land–atmosphere interactions can substantially influence regional climate simulations. Among these uncertainties, the surface exchange coefficient C_h is a critical parameter, controlling the total energy transported from the land surface to the atmosphere. Although it directly impacts the coupling strength between the surface and atmosphere, it has not been properly evaluated for regional climate models. This study assesses the representation of surface coupling strength in a stand-alone Noah-MP land surface model and in coupled 4-km Weather Research and Forecasting (WRF) model simulations. The data collected at eight FLUXNET sites of the Canadian Carbon Program and seven AMRIFLUX sites are used to evaluate the offline Noah-MP simulations. Nine of these FLUXNET sites are used for the evaluation of the coupled WRF simulations. These sites are categorized into three land use types: grassland, cropland, and forest. The surface exchange coefficients derived using three formulations in Noah-MP simulations are compared to those calculated from observations. Then, the default $C_{zil}=0$ and new canopy-height dependent C_{zil} are used in coupled WRF simulations over the spring and summer in 2006 to compare their effects on surface heat flux, temperature, and precipitation. When the new canopy-height dependent C_{zil} scheme is used, the simulated C_h exchange coefficient agrees better with observation and improves the daily maximum air temperature and heat flux simulation over grassland and cropland in the US Great Plains. Over grassland, the modeled C_h shows a different diurnal cycle than that for observed C_h , which makes WRF lag behind the observed diurnal cycle of sensible heat flux and temperature. The difference in precipitation between the two schemes is not as clear as the temperature difference because the impact of changing C_h is not local.

Keywords Surface exchange coefficient · Surface coupling strength · Surface fluxes · Land–atmosphere interaction

1 Introduction

Land–atmosphere interactions play important roles in weather and climate systems through the exchange of energy, moisture, and momentum between the atmosphere and land surface (Knist et al. 2017). Land–atmosphere coupling strength is the degree to which anomalies in land surface

states are transported to the atmosphere and hence impact atmospheric processes from an atmospheric perspective (Koster et al. 2006). Many observational studies have shown the importance of land–atmosphere coupling for regional weather and climate. LeMone et al. (2008) indicate that wetter soils can lead to higher evaporation and higher latent heat flux by affecting atmospheric heating rates, cloud formation, and therefore regional precipitation. Fischer et al. (2007) and Hirsch et al. (2014) have demonstrated that the land–atmosphere interaction impacts near surface temperature, humidity, cloud formation, rainfall generation, and other atmospheric processes through the modulation/partition of the exchange of latent heat and sensible heat between the land surface and atmosphere (Fischer et al. 2007; Hirsch et al. 2014; Kang et al. 2007; LeMone et al. 2008; Niyogi et al. 1999; Pielke 2001; Knist et al. 2017; Zheng et al. 2015).

The land–atmosphere coupling processes and their impacts on regional climate change have been investigated

✉ Yanping Li
Yanping.li@usask.ca

¹ CAS Key Laboratory of Regional Climate Environment for Temperate East Asia, Institute of Atmospheric Physics, Chinese Academy of Sciences (CAS), Beijing, China

² Global Institute for Water Security, University of Saskatchewan, 11 Innovation Boulevard, Saskatoon, SK S7N 3H5, Canada

³ National Center for Atmospheric Research, Boulder, CO, USA

in many observational and modeling studies, especially those involve soil moisture–temperature and soil moisture–precipitation feedbacks (Dirmeyer 2000; Guo and Dirmeyer 2013; Guo et al. 2006; Hirsch et al. 2014; Koster et al. 2003, 2004, 2006; Seneviratne et al. 2006, 2010). Understanding the feedbacks between land surfaces and the atmosphere can help improve weather and climate prediction in regional and global models (Barlage et al. 2015; Chang et al. 2009; Chen and Dudhia 2001; Chen and Zhang 2009; Kumar et al. 2014; Rasmussen et al. 2011; Trier et al. 2004, 2008). For land surface models (LSMs), determining a correct representation of the land–atmosphere coupling strength is challenging. Uncertainties in energy and water fluxes in LSMs arise from the choice of schemes used to represent land surface (Chen and Zhang 2009) and boundary layer processes (Sellers et al. 1997; Overgaard et al. 2006; Dickinson 2011), and from meteorological inputs (Santanello et al. 2009). Several studies of coupled atmosphere–ocean general circulation models (GCMs) have also demonstrated that the coupling strength between the land and atmosphere is highly dependent on model parameterizations. Therefore, an evaluation of simulated coupling strength against observation is desirable. (Koster et al. 2002, 2004, 2006; Guo et al. 2006).

Land–atmosphere coupling is a complex process that involves many aspects of the terrestrial–atmosphere system: soil moisture, aerodynamic resistance, stomatal resistance, flux partitioning, etc. Several metrics have been defined for quantifying the land–atmosphere coupling strength depending on the variables involved and the feedback processes addressed in global climate models and regional climate models, e.g. by Seneviratne et al. (2006, 2010), Decker et al. (2015), Lorenz et al. (2015) and Knist et al. (2017), and through diagnosis of observation and reanalysis, e.g., by Dirmeyer (2011), Miralles et al. (2012), etc. These methods mainly address the soil moisture–temperature feedback processes and on the time scale of days to months, though not all methods necessarily use the soil moisture variable explicitly in their formulas. In this study, we focus on the surface coupling strength involving the thermal roughness length that depends on the instantaneous atmospheric conditions (near surface wind speed, temperature difference between the surface and atmosphere) and the roughness of the land surface.

LeMone et al. (2008) and Chen and Zhang (2009) have indicated that the coupling strength in the bulk heat transfer equation between the land surface and the atmosphere can be quantified by the surface exchange coefficient C_h as it is the key factor for determining the amount of energy transferred from the surface to the lower atmosphere (a more detailed description of C_h is found in Sect. 2.1). Coupling strength depends on the exchange coefficient for different land-cover types and climate regimes. Chen and Zhang (2009) and Zheng et al. (2015) applied the bulk transfer

aerodynamic method in which C_h can be calculated from simulation and observation. Their studies call for a dynamic coupling strength in terms of the Zilitinkevich (1970) empirical coefficient C_{zil} , and the evaluation was only performed over a short time scale. How it works in a climate timescale remains unknown. Thus, evaluations of C_h in climate models are needed to investigate the effects of different formulations of the surface exchange coefficient on climate simulations. Several formulas represent C_h in the literature (Chen et al. 1997; Chen and Zhang 2009) as presented in Sect. 2, but their effects on land surface modeling have not been thoroughly investigated against observations.

The objectives of this study are to: (1) evaluate several C_h formulas in offline Noah-MP LSM against the C_h derived from long-term summer observations; (2) evaluate the simulated C_h with different formulas from high-resolution regional climate simulations (WRF) against the C_h derived from observations; and (3) assess the impacts of using a dynamic canopy-dependent C_h formula on WRF regional climate simulations.

This paper is organized as follows. Section 2 describes the datasets used and the experiment setups using the offline Noah-MP LSM and the coupled WRF model. Section 3 discusses the effect of land-coupling strength on both the stand-alone LSM and the WRF simulation. The conclusions and discussions are provided in Sect. 4.

2 Data and methods

This section describes the formulas of C_h , the FLUXNET observation dataset, as well as the experiment setup of the Noah-MP LSM and the WRF regional climate simulations. First, we evaluated the C_h coefficient from a recently-conducted regional climate simulation in the contiguous US against the C_h derived from FLUXNET Canada and Ameri-flux tower observations. Then, we tested several formulas of C_h and assessed the impacts of the coupling coefficients on surface fluxes (sensible heat flux and latent heat flux) within the Noah-MP offline model. Finally, we evaluated the impacts of the new canopy-dependent C_h on surface fluxes, temperature, and precipitation in a high-resolution regional climate simulation. For the comparison of temperature and precipitation for the coupled WRF simulation, we used PRISM data (PRISM Climate Group 2004) and WFDEI (Weedon et al. 2014) as benchmarks.

2.1 Land-atmospheric coupling method and the experiment design

In the original Noah LSM, the surface sensible (H) and latent (LH) heat fluxes are determined through the bulk transfer relations (Garrat 1992) as:

$$H = \rho C_p C_h |U| (\theta_s - \theta_a) \quad (1)$$

$$LH = \rho C_e |U| (q_s - q_a) \quad (2)$$

where ρ is the air density, C_p is the air heat capacity, $|U|$ is the wind speed, θ_a and q_a are the air potential temperature and the air specific humidity at the lowest model level or at a specific height above the ground, and θ_s and q_s are the surface temperature and the surface specific humidity. C_h and C_e are the surface exchange coefficient for sensible and latent heat fluxes and C_e is assumed to be equal to C_h . Hereafter, we focus on C_h . These equations have been discussed in several previous studies (Chen et al. 1997; Chen and Zhang 2009; Zheng et al. 2015). In the Noah-MP LSM, the ground surface is separated between vegetated canopy, vegetated ground, and the bare ground surface; hence, the surface energy balance is determined respectively (Niu et al. 2011). The sensible heat and latent heat flux formulas for these three surfaces use a similar form to Eqs. (1) and (2), although the surface relative humidity h_g is introduced in the vegetated and bare ground latent heat to characterize the availability of soil moisture (Niu et al. 2011, Appendix A).

C_h is determined by the Monin–Obukhov similarity theory as:

$$C_h = \frac{\kappa^2/R}{\left[\ln\left(\frac{z_a}{z_{om}}\right) - \psi_m\left(\frac{z_a}{L}\right) + \psi_m\left(\frac{z_{om}}{L}\right) \right] \left[\ln\left(\frac{z_a}{z_{or}}\right) - \psi_h\left(\frac{z_a}{L}\right) + \psi_h\left(\frac{z_{or}}{L}\right) \right]} \quad (3)$$

where L is the Monin–Obukhov length, Z_a is the height above the surface ground, R is the Prandtl number, and ψ_m and ψ_h are stability functions (Stull 1988). Also, in Eq. (3), Z_{or} is the roughness length for moisture and heat and Z_{om} for momentum, and they are assumed to be the same. Many studies (Chen and Zhang 2009; Brutsaert 1982; Sun and Mahrt 1995) have indicated that Z_{or} is different from Z_{om} because heat and momentum transfers are determined by different resistances and mechanisms in the roughness layer. Sun (1999) also found that Z_{or} has a much larger interday and diurnal variation depending on the factors involved in the bulk transfer formula (Eq. (1)), even over homogeneous surfaces (e.g., grassland). Zilitinkevich (1970) proposed a formula for Z_{or} :

$$Z_{or} = Z_{om} \exp\left(-k C_{zil} \sqrt{R_e}\right) \quad (4)$$

$$R_e = \frac{u_0^* Z_{om}}{\nu} \quad (5)$$

where $k=0.4$ is the von Kaman constant, R_e is the roughness Reynolds number, u_0^* is the friction velocity, and ν is the kinematic molecular viscosity, and an empirical coefficient C_{zil} . Chen et al. (1997) indicated that the C_{zil} values are

assumed to vary from 0.01 (strong coupling) to 1.0 (weak coupling). Zheng et al. (2015) also confirmed that a smaller C_{zil} results in stronger surface coupling. The default M–O option in Noah-MP LSM is the same as setting C_{zil} to 0, assuming $Z_{or} = Z_{om}$.

The Z_{or}/Z_{om} ratio, through the change of C_{zil} , can modulate surface heat fluxes. This ratio is more realistic than the treatment in the Monin–Obukhov option. Therefore, the specification of C_{zil} is expected to improve the model performance of surface fluxes. Chen and Zhang (2009) analyzed multi-year Ameriflux data and found that the C_{zil} values are vegetation-type dependent and that C_{zil} can be represented as a function of canopy height h (in meters):

$$C_{zil} = 10^{(-0.4h)}. \quad (6)$$

Chen and Zhang (2009) demonstrated that the canopy-height dependent C_{zil} formula (Eq. (6)) significantly improved the simulation results, especially in short vegetation sites.

2.2 FLUXNET data sets

FLUXNET, a global network of micrometeorological tower sites, uses eddy covariance methods to estimate the exchanges of carbon dioxide, water vapor, and energy between the atmosphere and terrestrial ecosystems. Both FLUXNET Canada and Ameriflux are part of FLUXNET. This study used data collected at 15 flux tower sites located in three biomes (grassland, cropland, and forest) and different climate zones, from FLUXNET Canada (CA-WP1, CA-Ca3, CA-Obs, CA-Qfo, CA-Ojp, CA-TP4) and Ameriflux (US-Bkg, US-Aud, US-Fpe, US-Wkg, US-Var, US-ARM, US-Bo1, US-NR1). Detailed information about the AmeriFlux network can be found at <http://public.ornl.gov/ameriflux/> and about CCP (Canadian Carbon Program) at https://fluxnet.ornl.gov/site_list/Network/3. Figure 1 shows the geographical locations of these sites, and Table 1 provides general information about them. Our goal is to explore the effect of the surface exchange coefficient C_h on the land-atmospheric surface coupling strength in regional climate models and compare them to uncoupled simulations using the approach by Chen and Zhang (2009).

2.3 Noah-MP LSM Offline modeling system

Noah-MP is a new-generation of LSM (Niu et al. 2011; Yang et al. 2011), which was developed to improve the performance of Noah LSM (Chen et al. 1996, 1997; Chen and Duhia 2001). It has been coupled to the community WRF weather and regional climate model (Barlage et al. 2015; Salamanca et al. 2018; Xu et al. 2018) and is also available as an offline 1-D model (e.g., Chen et al. 2016). Noah-MP has been widely used in regional climate models for

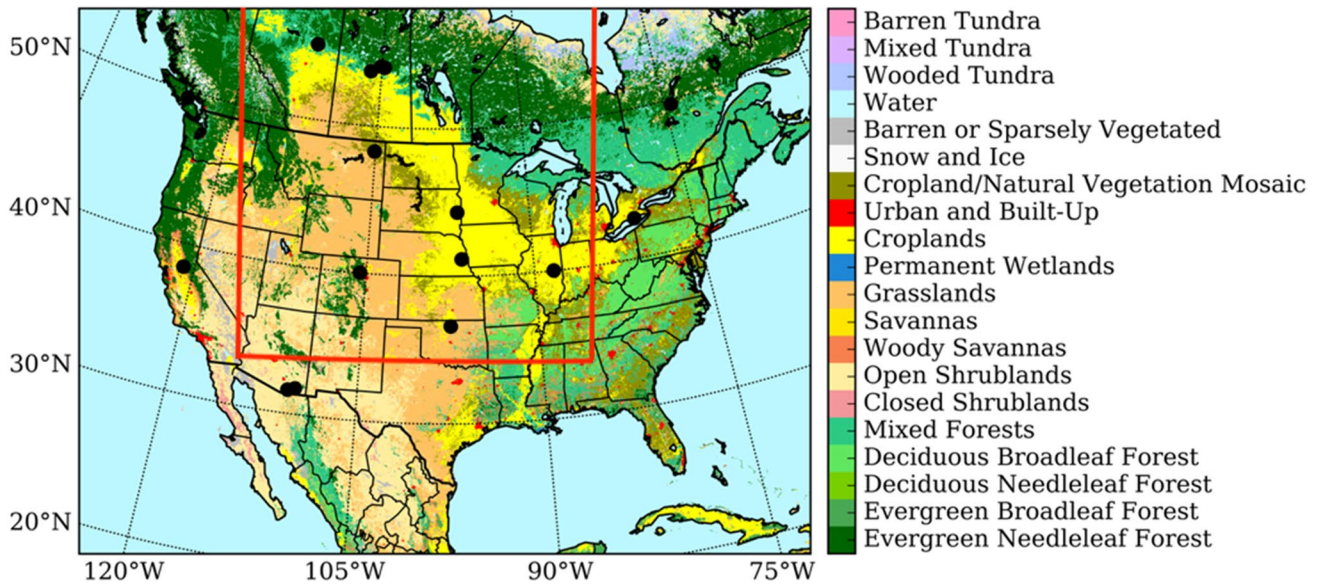


Fig. 1 Locations of 15 FLUXNET sites (in dark circles) selected for this study. The domain inside the red line is the smaller domain where coupled WRF simulations were conducted. Also shown is the distribution of vegetation based on the IGBP/MODIS land cover classification

Table 1 General information about 15 FLUXNET sites used in this study

| Site location | Latitude, longitude | Elevation (m) | Land-cover type | Canopy height (m) | Years of data used |
|---------------|---------------------|---------------|-----------------|-------------------|--------------------|
| US-Bkg | 44.35, -96.83 | 510 | Croplands | 0.2–0.4 | 2005–2007 |
| US-Aud | 31.59, -110.51 | 1469 | OSH | 0.1–0.2 | 2003–2007 |
| US-Fpe | 48.31, -105.10 | 634 | Grassland | 0.2–0.4 | 2001–2007 |
| US-Wkg | 31.74, -109.94 | 1531 | Grassland | 0.5 | 2005–2007 |
| US-Var | 38.41, -120.95 | 129 | WS | 0.55 ± 0.12 | 2001–2007 |
| US-ARM | 36.61, -97.49 | 311 | Croplands | 0–0.5 | 2003–2007 |
| US-Bo1 | 40.01, -88.29 | 219 | Croplands | 3.0 (mz) 0.9 (sb) | 2001–2007 |
| CA-WP1 | 54.95, -112.47 | 549 | WET | 3.4 | 2004–2007 |
| CA-Ca3 | 49.53, -124.90 | 153 | ENF | 7.6 | 2001–2007 |
| CA-Obs | 53.99, -105.12 | 598 | ENF | 9.4 | 2001–2007 |
| US-NR1 | 40.03, -105.55 | 3050 | ENF | 11.5 | 2001–2007 |
| CA-Qfo | 49.69, -74.34 | 390 | ENF | 13.8 | 2004–2007 |
| CA-Ojp | 53.92, -104.69 | 518 | ENF | 16.7 | 2001–2007 |
| CA-TP4 | 42.71, -80.36 | 219 | Mixed forest | 20.3 | 2002–2007 |
| CA-Oas | 53.63, -106.20 | 580 | DBF | 21.5 | 2001–2007 |

ENF evergreen needleleaf forests, DBF deciduous broadleaf forests, WET permanent wetland, WS wooded savannah

investigating the feedback between soil moisture and precipitation (the interaction between the land and atmosphere) (Barlage et al. 2015; Wan et al. 2017).

For this study, we chose the Noah-MP LSM (v3.6) to evaluate its C_h calculation. The Noah-MP LSM has two options to calculate C_h : one uses Monin–Obukhov (M–O) with identical roughness lengths for momentum (Z_{0m}) and heat (Z_{0r}), and the other uses different roughness lengths for Z_{0m} and Z_{0r} (Chen et al. 1997). Chen and Zhang (2009)

demonstrated that the canopy-height dependent C_{zil} formula (Eq. (6)) significantly improves the simulation results, especially in short vegetation sites.

In the offline Noah-MP simulations, we tested and compared three options for C_{zil} : the Noah-MP LSM original Monin–Obukhov, which uses $C_{zil} = 0$; a constant $C_{zil} = 0.1$, and the canopy-height dependent scheme according to Eq. (6). The model simulated C_h is compared with observation-derived C_h from the FLUXNET sites.

2.4 WRF model and domain configuration

The weather research and forecasting (WRF) model was configured with 4-km horizontal grid spacing that permits convection and resolves mesoscale orography covering large parts of North America (1360 by 1016 grid points, Fig. 1) (Rasmussen and Liu 2017; Liu et al. 2017). The WRF model was used to directly downscale the European Centre for Medium-Range Weather Forecast Interim Reanalysis (ERA-Interim) (Dee et al. 2011) data for the period from October 2000 to September 2013 to generate a high-resolution regional climate simulation (WRF-CONUS). The WRF-CONUS dataset has been used for several regional climate studies on, regarding convective precipitation (Prein et al. 2016; Rasmussen et al. 2017; Scaff et al. 2019), snow hydrology (Musselman et al. 2017, 2018), and extreme heat waves (Raghavendra et al. 2019; Zhang et al. 2018). The first three months are treated as a spin-up period and not included in the analysis. The output from WRF-CONUS is used as forcing for offline simulations using Noah-MP with different C_{zil} formulas to compare the impact of C_{zil} schemes on C_h , surface temperature, and heat flux simulation.

For our coupled WRF simulation with different C_{zil} formulations, the simulation was performed over a smaller domain over the central part of the continent, as shown in the boxed region in Fig. 1, for the period from 2006 to 2007. In the default simulation (WRF-CTL), the parameterization schemes employed are identical to those described in Liu et al. (2017). To investigate the impacts of coupling strength on WRF-Noah-MP model simulations, another simulation with the canopy-height dependent formula $C_{zil} = 10^{(-0.4h)}$ (WRF-CZIL) is performed over the small domain. WRF-CZIL uses the same physics scheme as Liu et al. (2017) except that in the Noah-MP LSM the new C_{zil} formulation (dependent on canopy height, Eq. (6)) replaces the default M–O scheme (equivalent to $C_{zil} = 0$). The coupled simulations (WRF-CTL and WRF-CZIL) over the small domain were initialized at 0000 UTC 1 Feb 2006 and ended at 0000 UTC 1 Sep 2007. The first month was treated as a spin-up period.

3 Results

3.1 Impact of the coupling strength on the offline Noah-MP LSM simulation

C_h can be directly derived from flux observations using the method from Chen and Zhang (2009). Instruments at FLUXNET sites directly provide sensible heat H and $|U|$; θ_a and θ_s are calculated from observed air temperature and outgoing longwave radiation flux. C_h is calculated

using 30-min data by the bulk transfer formula in Eq. (1) and then averaged from 1000 to 1500 local time to obtain midday values. Figure 2 shows midday C_h calculated by FLUXNET data and offline Noah-MP experiments using the FLUXNET data for each station in Table 1 and averaged for spring and summer. Compared to the midday observation-derived C_h , the modeled C_h values from the default run are overestimated for all sites. Especially the positive bias of C_h in short vegetation (grassland and cropland: US-Bkg to Ca-WP1) is larger than in forest sites. This result agrees with Chen and Zhang (2009) in that Noah LSM overestimates the surface coupling strength in short vegetation sites and provides too much water vapor, while the LSM reasonably captures the coupling for forest sites. In the simulations with $C_{zil} = 0.1$, the C_h values decrease for all the sites. Compared to the observation, $C_{zil} = 0.1$ improves C_h over short vegetation but still overestimates it, while for the forest sites the C_h values are underestimated. Thus, based on the simulation results, a constant C_{zil} value cannot represent the strong dependency of C_h on vegetation types with different canopy heights in Noah-MP LSM. Using canopy-height dependent C_{zil} , as in Eq. (6), significantly improves the midday C_h values in short vegetation sites with good agreement with observation, while in forest sites, the simulated C_h are still overestimated but reasonable for summer. The above analysis demonstrates that adjusting the C_{zil} values can substantially improve the land-atmospheric coupling strength for different land cover types, especially for short vegetation sites. Except for the site US-NR1, all offline simulations show a much narrower range for C_h compared to observation, meaning that Noah-MP produces a smaller diurnal cycle of C_h than observation in offline simulations. Any factors and observation uncertainties that affect the variables in the bulk transfer formula (Eq. (1)) can cause large changes and variations in C_h derived from FLUXNET data.

Figures 3, 4, and 5 show the diurnal surface heat fluxes (averaged from 2001 to 2007) from FLUXNET observation and offline Noah-MP simulations forced by FLUXNET data over all sites, with the same land cover for three different land covers (grassland, cropland, and forest). There are small differences (underestimations) between modeled LH using three formulas ($C_{zil} = 0, 0.1$ and h-dependent) and observed LH over the three land cover types. Large differences (overestimations) are found in H among the three simulations and observations. The changes are small in LH among the three formulas because the LH is also strongly affected by moisture availability besides the exchange coefficient. Compared to the observed H, both the default and $C_{zil} = 0.1$ experiment overestimate H over cropland and grassland at midday, confirming again that the surface coupling strength is too strong for cropland and grassland sites in the daytime. Figure 3 shows that over

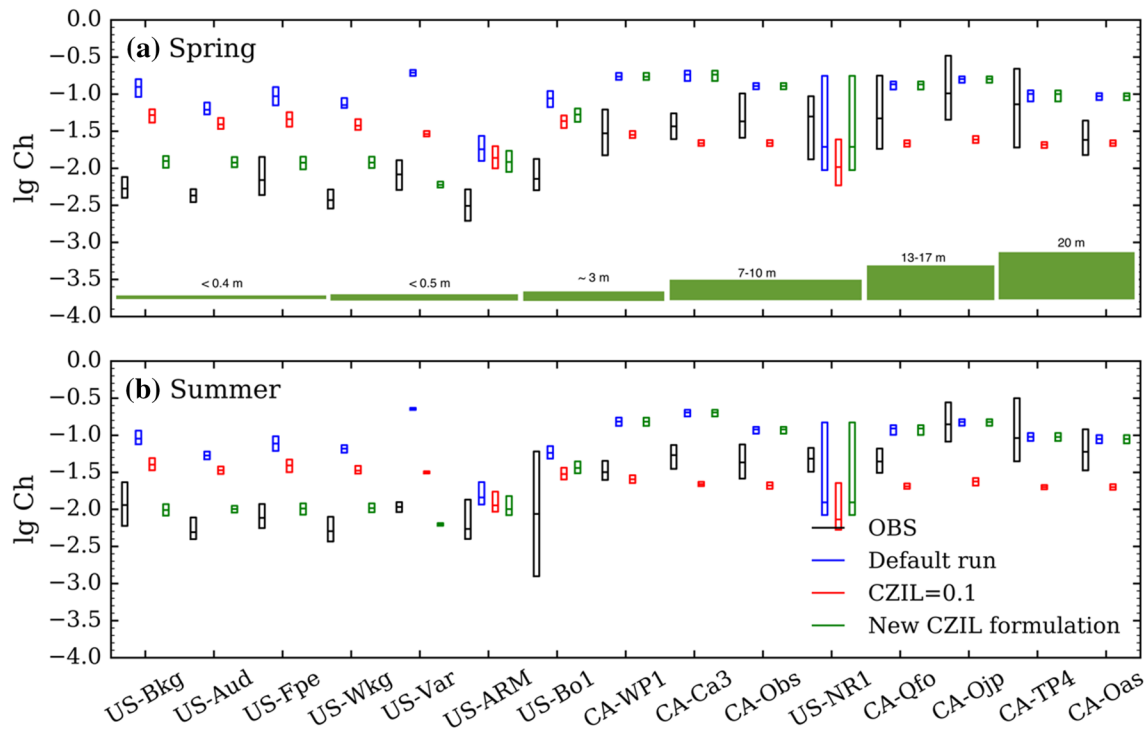


Fig. 2 C_h (plotted at \log_{10} scale) derived from FLUXNET observations, calculated by the Noah-MP LSM using default M–O scheme run, CZIL=0.1, and $C_{zi}(h)$ relationship of Eq. (6) for different land-cover types. These are midday (1000–1500 LST) values and averaged

for spring (March–April–May) and summer (June–July–August). The median values of spring (summer) average C_h are represented by middle lines. The bars comprise 75% of all midday values C_h for spring (summer) for each site

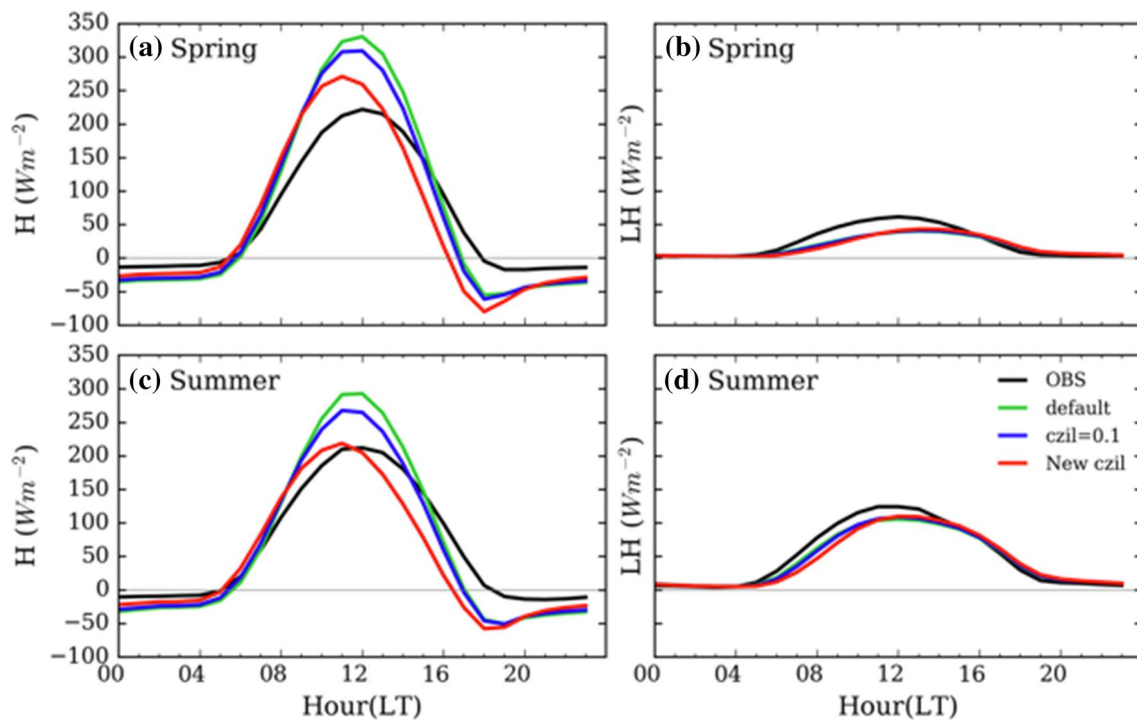


Fig. 3 Comparisons of averaged surface sensible heat flux and latent heat flux between observation and offline experiments over grassland sites

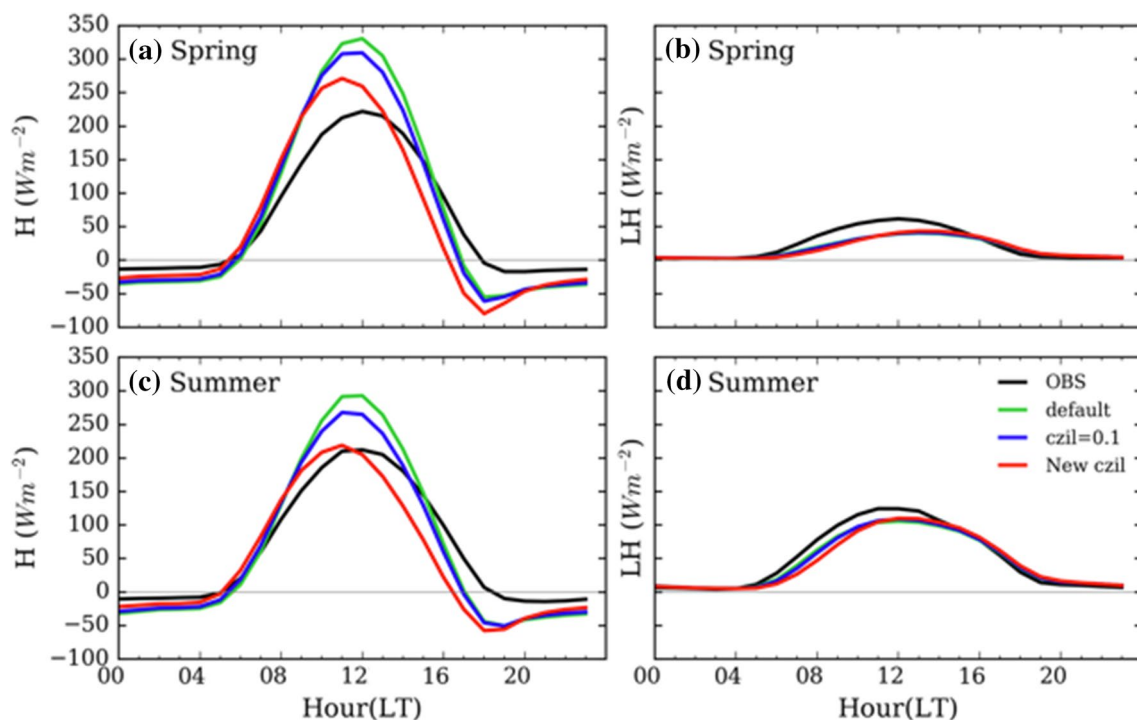


Fig. 4 Comparisons of averaged surface sensible heat flux and latent heat flux between observation and offline experiments over cropland sites

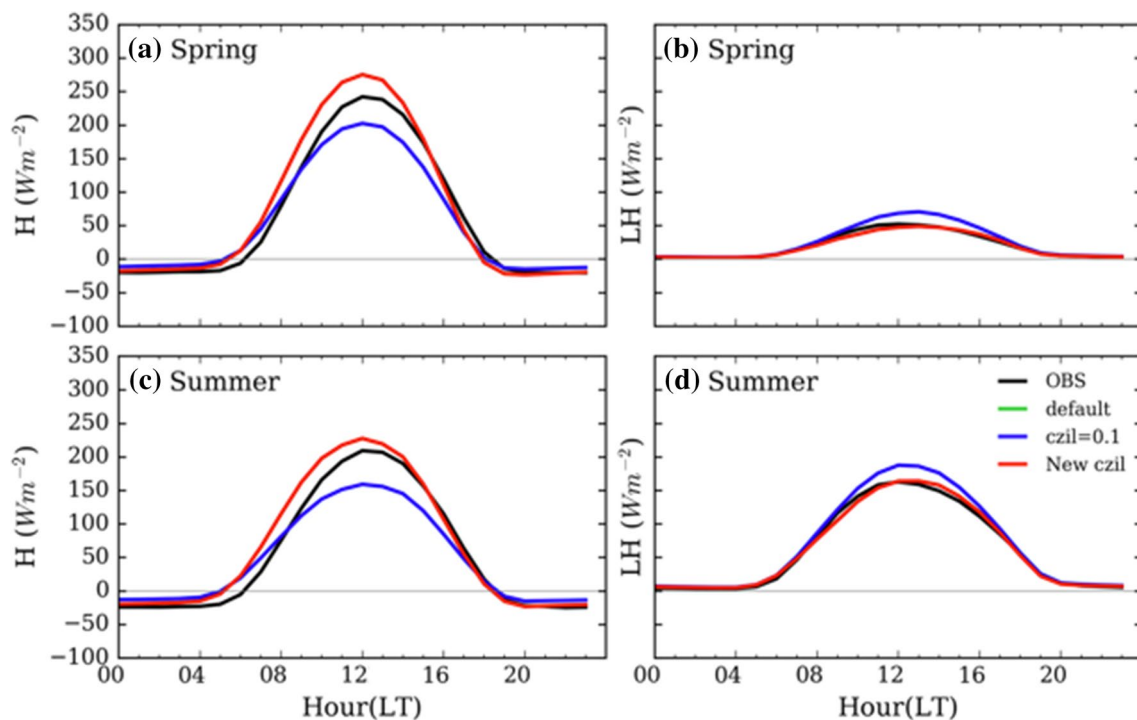


Fig. 5 Comparisons of averaged surface sensible heat flux and latent heat flux between observation and offline experiments over forest sites

grassland the $C_{zil}(h)$ simulation reproduces the observed H maximum value. However, the simulated H peaks earlier than in the observation. This is due to the thermal

difference between the surface and atmosphere peaking earlier in the $C_{zil}(h)$ simulation. $C_{zil}(h)$ decreases C_h significantly over grassland compared to the default and $C_{zil} = 0.1$

simulations and is closer to the mean observed C_h value at midday (not shown). However, the observed C_h peaks around early morning and late afternoon over the grassland sites, whereas the simulated C_h (default, $C_h=0.1$, $C_{zil}(h)$) peaks at midday. Large observed C_h in the morning corresponds to a large H with a small thermal gradient. The significant decrease in C_h for the $C_{zil}(h)$ simulation requires a larger temperature difference between the land surface and atmosphere in the morning to match the observed H . This larger thermal difference causes larger H in the early morning as the simulated C_h increases with local solar time, hence the earlier peak time for H than the other two simulations and the observation. Through the investigation of momentum and thermal roughness length over grassland, Sun (1999) found nearly constant values for momentum roughness length but a large diurnal variation of thermal roughness length. Sun also found that when the surface wind is weak, the aerodynamic temperature used in the bulk flux equation (Eq. (1)) deviates far from the surface radiation temperature and that apparent counter thermal gradient heat transport occurs under such conditions. Over the grassland sites in this study, the weakest surface wind speeds occur during the transitional periods of morning and evening, which coincide with the large C_h values over the grassland and some cropland FLUXNET sites. To better simulate the sensible heat flux and temperature diurnal cycle over grasslands, more studies are warranted to investigate the diurnal variation of thermal roughness length and surface exchange coefficient C_h over grasslands.

Figure 4 shows that although the simulation with the canopy height dependent $C_{zil}(h)$ still overestimates H for cropland, it matches the observed H better within a reasonable range. The changes in H from the default to $C_{zil}(h)$ are relatively small in spring compared to summer. The new C_{zil} formula reduces the positive bias of H to about 50% of that of the default simulation. There are almost no differences in the simulated LHs for the three formulas, all of which show large negative biases for both seasons.

For the forest sites in Fig. 5, both default and $C_{zil}=0.1$ simulations underestimate H , but the new C_{zil} simulations slightly overestimate H and are closer to the observed value than the other two simulations. In general, the coupling strength is too weak for forest sites in both the default and $C_{zil}=0.1$ experiments. For forest sites, there is not much difference between the default and new C_{zil} in H , since a high canopy will yield a C_{zil} close to 0 and make it nearly identical to the default C_h scheme, overestimating H at the same scale. Yet a constant $C_{zil}=0.1$ underestimates H and overestimates LH fluxes in forest sites. The underestimation of H by $C_{zil}=0.1$ is expected with a smaller C_h as less heat is transferred from the surface to the atmosphere, resulting in a higher skin temperature. The increase of skin temperature

enhances the evaporation from the ground and canopy. For all the cases with a smaller C_h ($C_{zil}(h)$ for grassland and cropland, and $C_{zil}=0.1$ for forest), H decreases substantially compared to cases with a larger C_h (default for grassland, cropland, and $C_{zil}(h)$, and default for forest). Although there is a large decrease of H and increase of skin temperature caused by a smaller C_h value, the changes in LH over grassland and cropland are negligible. The simulated changes in LH over forest sites are larger due to their larger soil moisture availability and smaller stomatal resistance, which play an important role in controlling moisture flux.

3.2 Impact of the coupling strength on the coupled WRF model

As the 13-year 4-km WRF-CONUS simulation does not use the new C_{zil} method, we conducted another set of experiments over a smaller domain using the identical configuration of WRF-CONUS and with both the default and a new $C_{zil}(h)$ method, known as WRF-CTL and WRF-CZIL, respectively. The simulation period for WRF-CZIL and WRF-CTL is from February 1, 2006 to September 1, 2007. In order to compare the performance of different C_{zil} formulas in the coupled model, the simulation results of both WRF-CTL (equivalent to $C_{zil}=0$) and WRF-CZIL ($C_{zil}(h)$) are analyzed. Figure 6 shows the C_h derived from observations and calculated by both WRF-CTL and WRF-CZIL run using the $C_{zil}(h)$ relationship of Eq. (6) (WRF-CZIL) for the nine FLUXNET sites through spring and summer for 2006 and 2007. Compared to observation-derived values, the WRF C_h has a much smaller range over all the sites regardless of scheme. As discussed in Sect. 3.1, the C_h derived from FLUXNET shows much larger diurnal variability. The WRF-CTL results overestimate C_h for short vegetation, while for the forest sites, the simulated C_h is very close to the observation-derived values. Using canopy height dependent C_{zil} , the WRF-CZIL simulation results slightly improve the C_h in short vegetation sites while matched with the observations over forest sites. WRF-CZIL with improved C_h produces better simulated mean air temperature results (Fig. 6). The WRF-CTL simulated temperature bias is generally more than 5 degrees in spring and summer for short vegetation; the new C_{zil} scheme cools down the warm bias by about 2° in general.

Figures 7, 8 and 9 present the impacts of the coupling strength through applying the $C_{zil}(h)$ formula to heat fluxes in coupled WRF simulations over three types of land surface. Figure 7 shows that in grassland sites during spring and summer the WRF-CZIL experiment improves the simulation of H at midday over WRF-CTL, although both overestimate H compared to observation. Both WRF-CTL and WRF-CZIL overestimate LH compared to observation with little difference between the two simulations. Unlike the

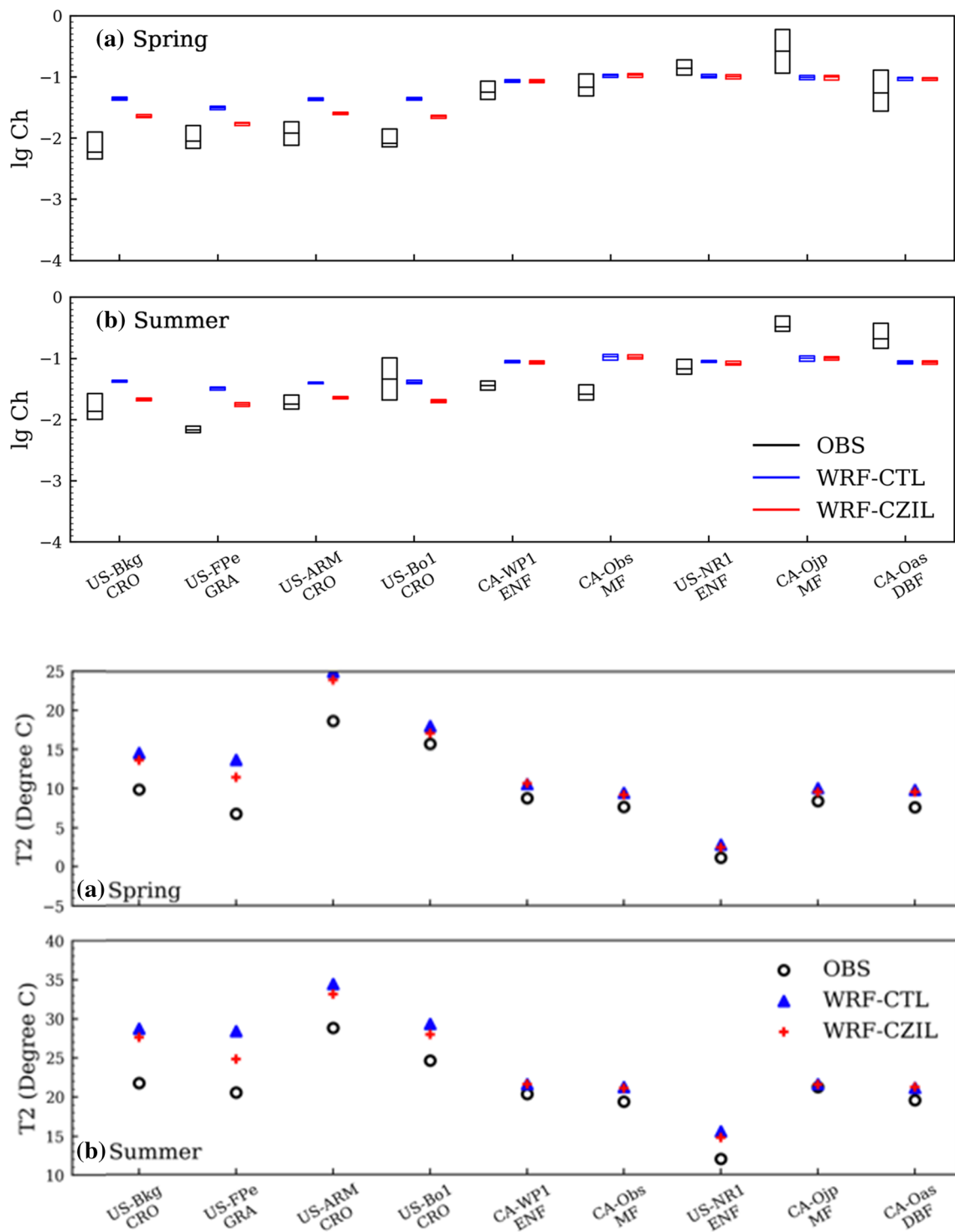


Fig. 6 C_h (top, plotted at \log_{10} scale) and T_2 (bottom) derived from FLUXNET observations, those calculated from two coupled WRF simulations (WRF-CTL and WRF-CZIL). C_h values are midday (1000–1500 LT) values and averaged for spring (March–April–May)

and summer (June–July–August) in 2006 and 2007. The median values of spring (summer) average C_h are represented by middle lines. The bars comprise 75% of all midday values C_h for spring (summer) for each site

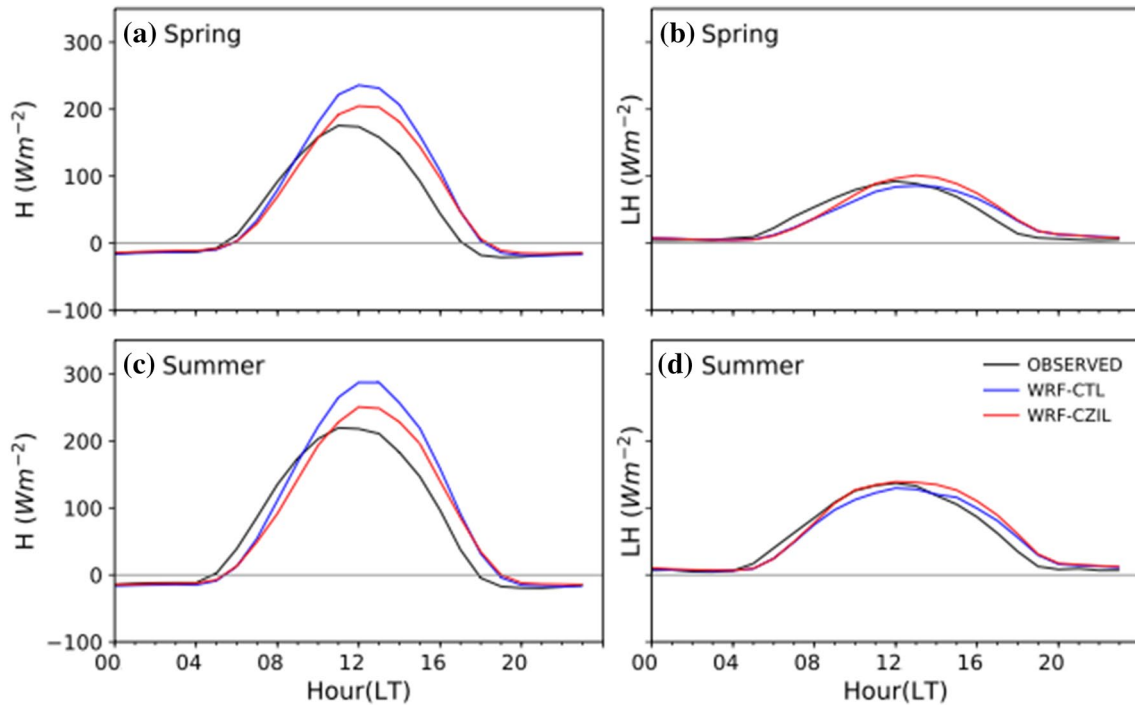


Fig. 7 Comparisons of averaged surface sensible heat flux and latent heat flux between observation and coupled WRF model results over grassland sites

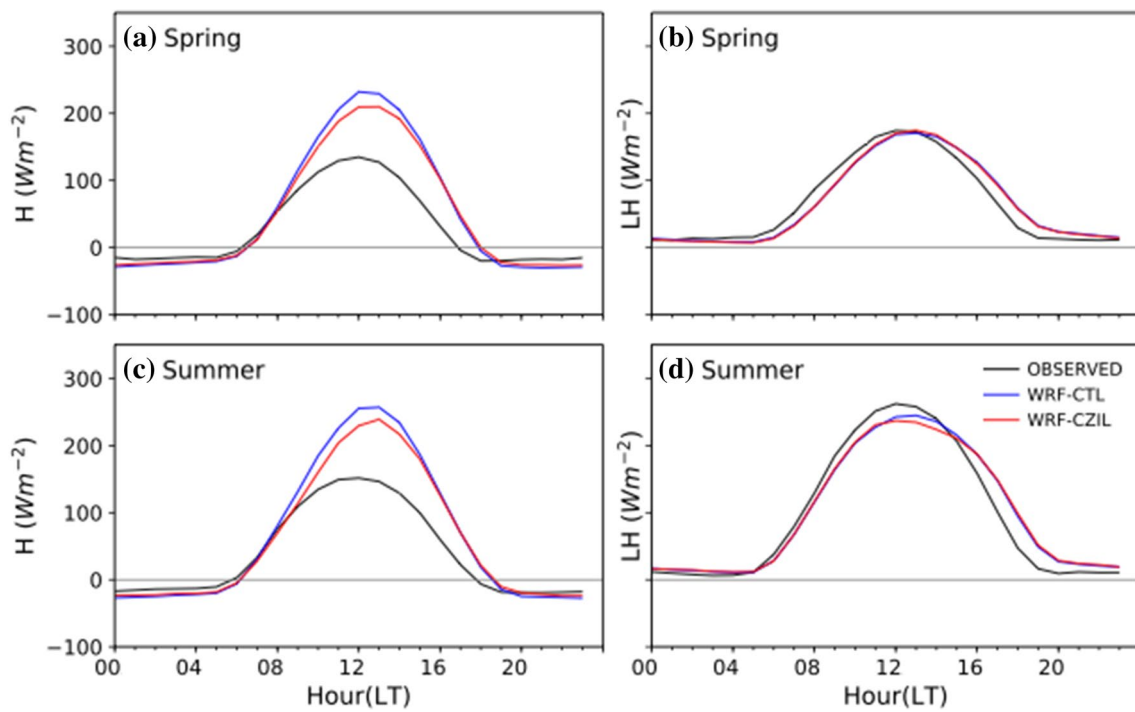


Fig. 8 Comparisons of averaged surface sensible heat flux and latent heat flux between observation and coupled WRF model results over cropland sites

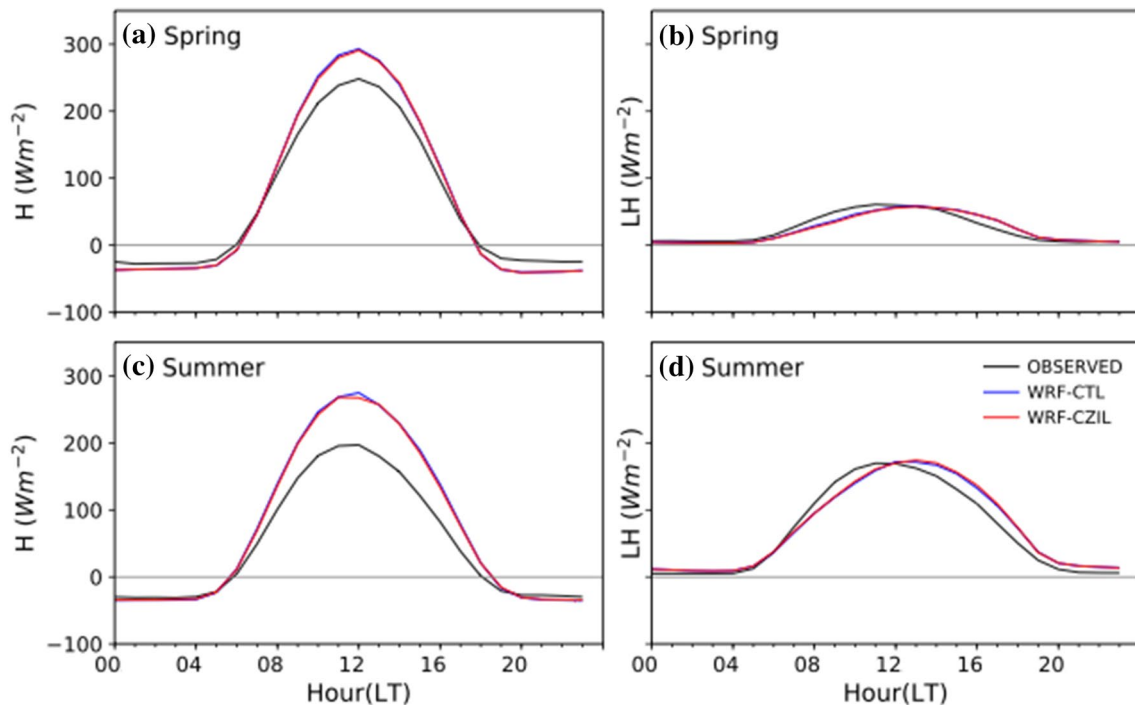


Fig. 9 Comparisons of averaged surface sensible heat flux and latent heat flux between observation and coupled WRF model results over forest sites

offline Noah-MP simulation in which the simulated H peaks earlier than in observation, the coupled simulation shows a delayed peak of H compared to FLUXNET observation. This delay is related to a much more gradual rise of skin temperature in the morning in both WRF-CTL and WRF-CZIL compared to observation. In the WRF-CTL simulation, the mean C_h is larger than the observed value. However, in the early morning the observed C_h value is as large as the C_h in WRF-CTL, in which the minimum value occurs early in the morning (Fig. 10). The temperature and skin temperature in the observation start to rise at an earlier local time than in both the WRF-CTL and WRF-CZIL simulations, which is consistent with the earlier rise of H in the observation. This delayed rise of H and temperature in the early morning in the WRF simulation contrasts with the offline simulation using Noah-MP, which produces an earlier peak of H than observation. The utilization of the new C_{zil} formula mainly decreases the peak magnitude of H and surface temperature and has no effects on the nighttime minimum surface temperature (not shown). WRF-CTL produces a diurnal range of surface temperature slightly less than observation. The new C_{zil} decreases the diurnal range of temperature relative to WRF-CTL and observation. In other words, a higher value of C_h in the early morning and in the evening in WRF-CZIL would improve the simulation of H and surface temperature in WRF-CZIL over grasslands.

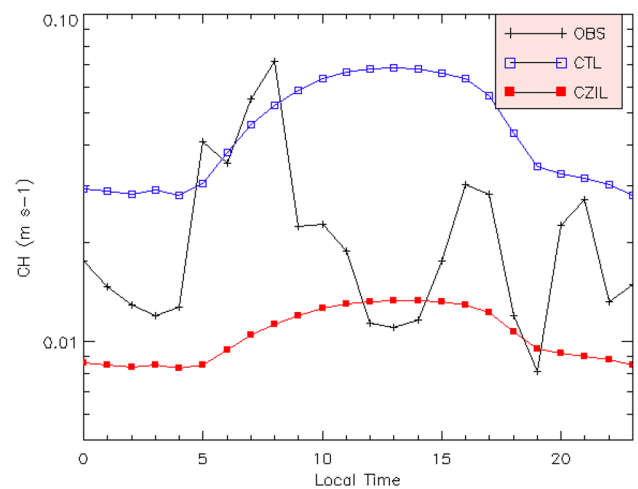


Fig. 10 The diurnal cycle of C_h from site US-Fpe (grassland) from observation during summer (JJA) and those from WRF-CTL and WRF-CZIL schemes

For cropland sites, as shown in Fig. 8, WRF-CTL and WRF-CZIL results are very similar in spring and summer. Both overestimate the observed H in midday by more than 100 Wm^{-2} . WRF-CZIL improves the H value and slightly reduces the positive bias relative to observed values compared to WRF-CTL. The C_h values in WRF-CTL are generally larger than in observation for the cropland sites. The C_h

values in WRF-CZIL are generally less than in observation, as shown in Fig. 6. The positive bias of H in the daytime in WRF-CZIL with a smaller C_h is due to the fact that the simulated skin temperature in WRF-CZIL at midday is much larger than in observation, which more than compensates for the effects of the reduced C_h . Compared to the offline simulation (Fig. 4), both WRF-CTL and WRF-CZIL simulate better LH, greatly reducing the negative bias in the simulated LH in the offline simulations. These better results for LH compared to offline simulations, however, are caused by a large warm bias in skin temperature (not shown) in both WRF-CTL and WRF-CZIL.

Over forest sites, WRF-CTL and WRF-CZIL produce similar H and LH in both spring and summer, as shown in Fig. 9. Because C_{zil} is close to 0 (default) for the canopy height of forest sites, according to Eq. (6). WRF-CTL and WRF-CZIL both overestimate H compared to observation. Figures 7, 8, and 9 show that the WRF-CZIL simulations agree better with observation in terms of H, while the coupling strength does not affect the LH much over all the FLUXNET sites, especially for the spring season. Compared to WRF-CTL, the WRF-CZIL using the $C_{zil}(h)$ relation can reduce the coupling strength in short vegetation sites, which brings the H simulation closer to observation for grassland and cropland during daytime. C_h improved by WRF-CZIL leads to better simulated mean 2-m air temperature results over grassland (Fig. 6). The WRF-CTL temperature bias is generally more than 5° in spring and summer for short vegetation, while the new C_{zil} scheme reduces the warm bias by about 2° in general.

Figures 11, 12 compare the spatial distribution of simulated daily maximum surface temperature (T_{max}) compared to PRISM in the US and to WFDEI in Canada in spring and summer for 2006 and 2007. Figure 11 shows that the spring T_{max} distribution simulated by WRF-CTL has a positive bias in the high plains centered over the Dakotas, Nebraska, Kansas, and Oklahoma, which are covered mostly by grasslands and croplands. WRF-CZIL reduces the warm bias in the region, especially over grassland. WRF-CTL also simulates cold biases over the grasslands close to the Rocky Mountains. WRF-CZIL enhances the cold bias by WRF-CTL over this region. Figure 12 shows that the general pattern of T_{max} bias during summer is similar to the pattern during spring for both WRF-CTL and WRF-CZIL. The summer T_{max} bias pattern shows a small shift toward the east relative to spring. WRF-CZIL reduces the warm bias in the eastern part of the central plains and worsens the cold bias in the grasslands close to the Rockies. Because the new C_{zil} scheme reduces C_h over short vegetation canopy, WRF-CZIL generally decreases the daily maximum temperature over the domain compared to WRF-CTL, since grassland and cropland are the dominant land use types in the domain.

Figures 13, 14 show the daily minimum temperature (T_{min}) from PRISM/WFDEI, WRF-CTL, and WRF-CZIL. WRF-CTL produces a warm bias in the whole domain, with the larger bias centering on the Great Plains for both spring and summer. There is a cold bias belt following the forest distribution in western Canada in both seasons. The WRF-CZIL simulation produces a very similar pattern with an enhanced warm bias over croplands in Illinois, Wisconsin, and Iowa. A nighttime temperature warm bias is the main contributor to the warm bias in daily mean temperature in WRF over the Great Plains.

Figures 15, 16 show the WRF precipitation simulation comparison with PRISM/WFDEI for spring and summer. The indirect impacts of the surface exchange coefficient on precipitation involve many processes, are nonlocal, and are not as clear as those for temperature. In Fig. 15, WRF-CTL produces a dry bias in the southeast domain that fades northwestward into the central plains and a wet bias over the cropland region during spring. The $C_{zil}(h)$ simulation enhances the wet bias over the cropland region in Missouri and Illinois. This region is warm during spring and downwind of the grassland region, where new C_{zil} increases LH and evaporation in the WRF-CTL simulation. Figure 16 shows that the precipitation pattern and changes in summer are more complex compared to spring. Observation shows a main precipitation region extending from Oklahoma (around 100° W) northeastward to Lake Michigan. WRF-CTL produces a wet bias of 4–5 mm/day in the forests of Minnesota and Wisconsin and in southwestern Ontario largely to the north/northeast of the observed main precipitation regions. WRF-CZIL tends to reduce this wet bias in WRF-CTL over the region and mitigate the dry bias in the cropland in WRF-CTL over the main precipitation area in the observation. In other words, compared to WRF-CTL, WRF-CZIL produces more precipitation over grassland and cropland in the main precipitation region in observation. WRF-CZIL also reduces precipitation in the forest zone north of the above region. WRF-CTL produces a wet bias of 2–3 mm/day near Wyoming and Nebraska and a dry bias to the east. WRF-CZIL seems to reduce these biases, which is consistent with the fact that WRF-CZIL has a lower C_h during daytime and simulates a lower maximum temperature over the grasslands close to the Rockies.

4 Discussion and conclusions

In this study, the impact of land-atmospheric coupling was assessed using an offline Noah-MP LSM and coupled WRF-Noah-MP model for selected FLUXNET sites and over the central US and Canada. Three formulas calculating the surface exchange coefficient C_h , including a canopy height dependent formula, were tested using the Noah-MP offline mode with observational forcing from the selected

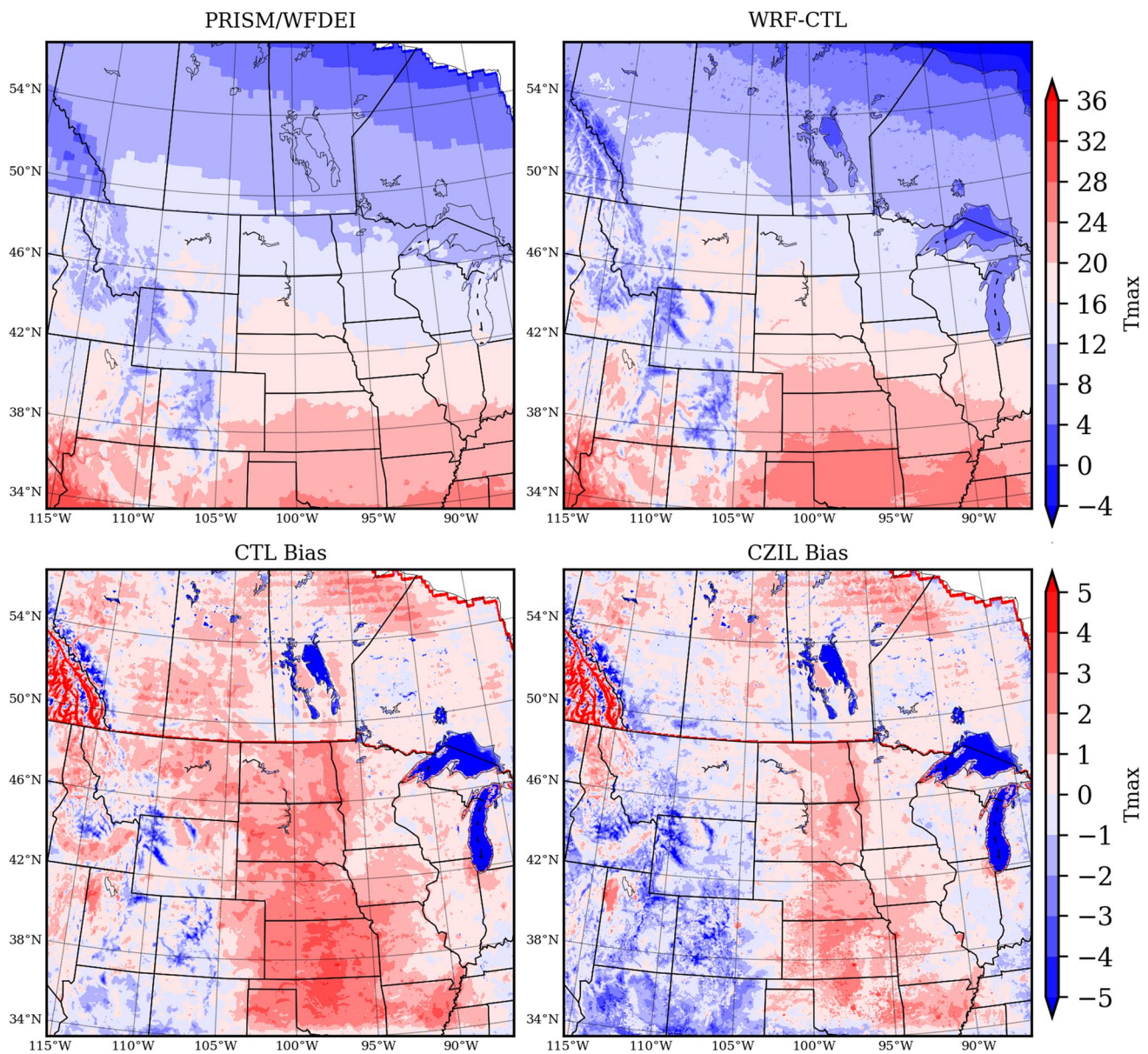


Fig. 11 Comparisons of T_{\max} from PRISM/WFDEI and coupled WRF model results in spring (MAM) of 2006, 2007. The top row shows the observation and WRF-CTL in degree Celsius. The bottom row shows the WRF-CTL and WRF-CZIL Bias in degree Celsius

FLUXNET sites. The default and new C_{zil} formulas were tested in WRF-Noah-MP coupled runs. The impacts of two C_{zil} formulas on the land–atmosphere interaction were studied through analysis of energy fluxes and surface temperature, and precipitation for spring and summer during 2006–2007.

The offline Noah-MP single point simulations forced by FLUXNET data with various coupling strength formulas show substantial differences in simulated C_h , as well as in surface energy fluxes, especially in sensible heat H . The default option, equivalent to $C_{zil} = 0$, overestimates C_h in all sites in both spring and summer. This leads to more energy

transferred as sensible heat flux over short vegetation, resulting in more over-coupling between land and atmosphere than in observation. The constant $C_{zil} = 0.1$ scheme reduces the positive C_h bias simulated by default over short vegetation and underestimates C_h over tall vegetation. The overestimation of the surface exchange coefficient by the constant C_{zil} over cropland and grassland is still evident, and so is the underestimation for forest sites. Finally, the new C_{zil} simulation produces the least mean C_h bias in short vegetation with decent results in tall vegetation, resulting in a small positive bias in H and a reasonably good estimation of LH for grassland and forest.

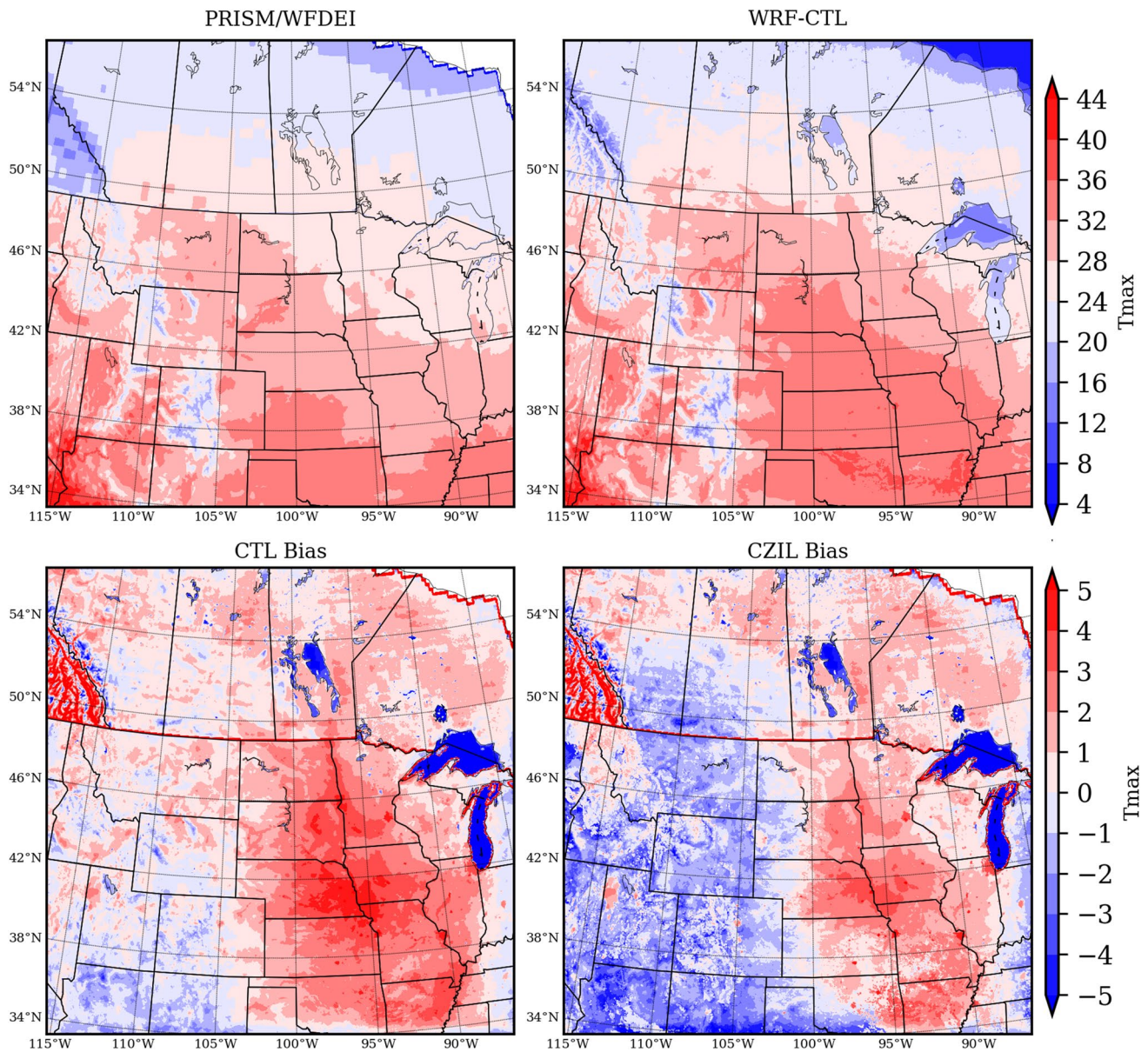


Fig. 12 Same as in Fig. 11, except for summer (JJA)

The C_h estimated using the bulk formula over grasslands shows a different diurnal cycle than both in Noah-MP and WRF. In both models, the diurnal cycle of C_h at each site shows a diurnal cycle following the temperature diurnal cycle. The observed C_h over grassland sites and some cropland sites shows a maximum near early morning and late afternoon (Fig. 10). The observed C_h over forest sites shows a varied pattern but resembles those from the model with the maximum during the daytime. This diurnal variation of C_h causes the offline Noah-MP and WRF-CZIL simulations to fail to capture the peak time for H over grassland. All the variables in the bulk formula in Eq. (1) can cause uncertainty and variation in C_h for grassland. Sun (1999) pointed

out that the aerodynamic temperature (the effective temperature for heat exchange between the surface and atmosphere when C_h is fixed in Eq. (1) and $Z_{or} = Z_{om}$) is higher than the radiative temperature when the wind speed is slow, which is the case for grassland sites in the early morning and late afternoon. A higher aerodynamic temperature is equivalent to a higher C_h using surface radiation temperature in Eq. (1).

The results from coupled WRF Noah-MP simulations with two coupling strength treatments, WRF-CTL and WRF-CZIL, differ in terms of H and LH. The changes caused by the different choices of C_{zil} schemes are smaller for the coupled runs compared to offline simulations. The C_h simulated by both schemes shows less variability than that

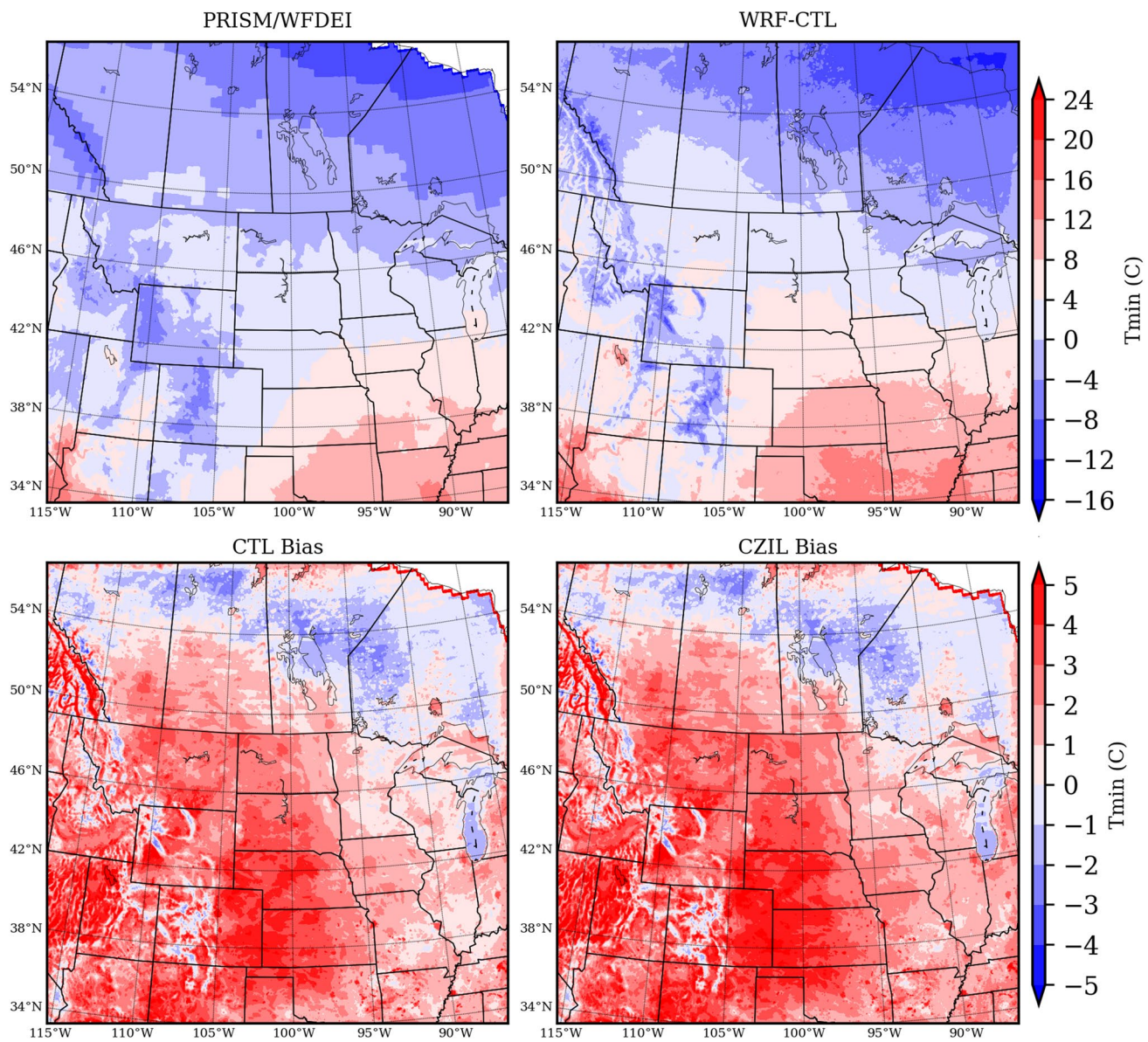


Fig. 13 Comparisons of T_{\min} from PRISM/WFDEI and coupled WRF model results in spring (MAM) of 2006, 2007. The top row shows the observation and WRF-CTL in degree Celsius. The bottom row shows the WRF-CTL and WRF-CZIL Bias in degree Celsius

derived from observation and that from offline Noah-MP results forced by FLUXNET in Sect. 3.1, suggesting that uncertainty from the measurement and representation of the related variables in Eq. (1) may introduce uncertainty of the exchange coefficient. The C_h simulated by WRF-CTL shows a constant positive bias over short vegetation and is close to the C_h for observation over forest in both spring and summer. WRF-CZIL improves the C_h over short vegetation while keeping a reasonably good estimation over tall vegetation. The two schemes show substantial differences in sensible heat and only small differences in latent heat. WRF-CZIL

reduces the strong positive midday sensible heat bias by as much as 100 Wm^{-2} , particularly in summer over cropland. For forest sites, the improvement in simulated sensible heat is not significant.

The WRF-CZIL simulation reduces the warm bias in 2-m air temperature in the WRF-CTL simulation by $2^\circ\text{--}3^\circ$ over short vegetation sites, suggesting the key role of land-atmosphere interaction in impacting local climate through surface coupling strength. These results provide solid evidence for diagnosing the warm bias that appears in summer over the North Great Plains in the CONUS simulation (Liu et al.

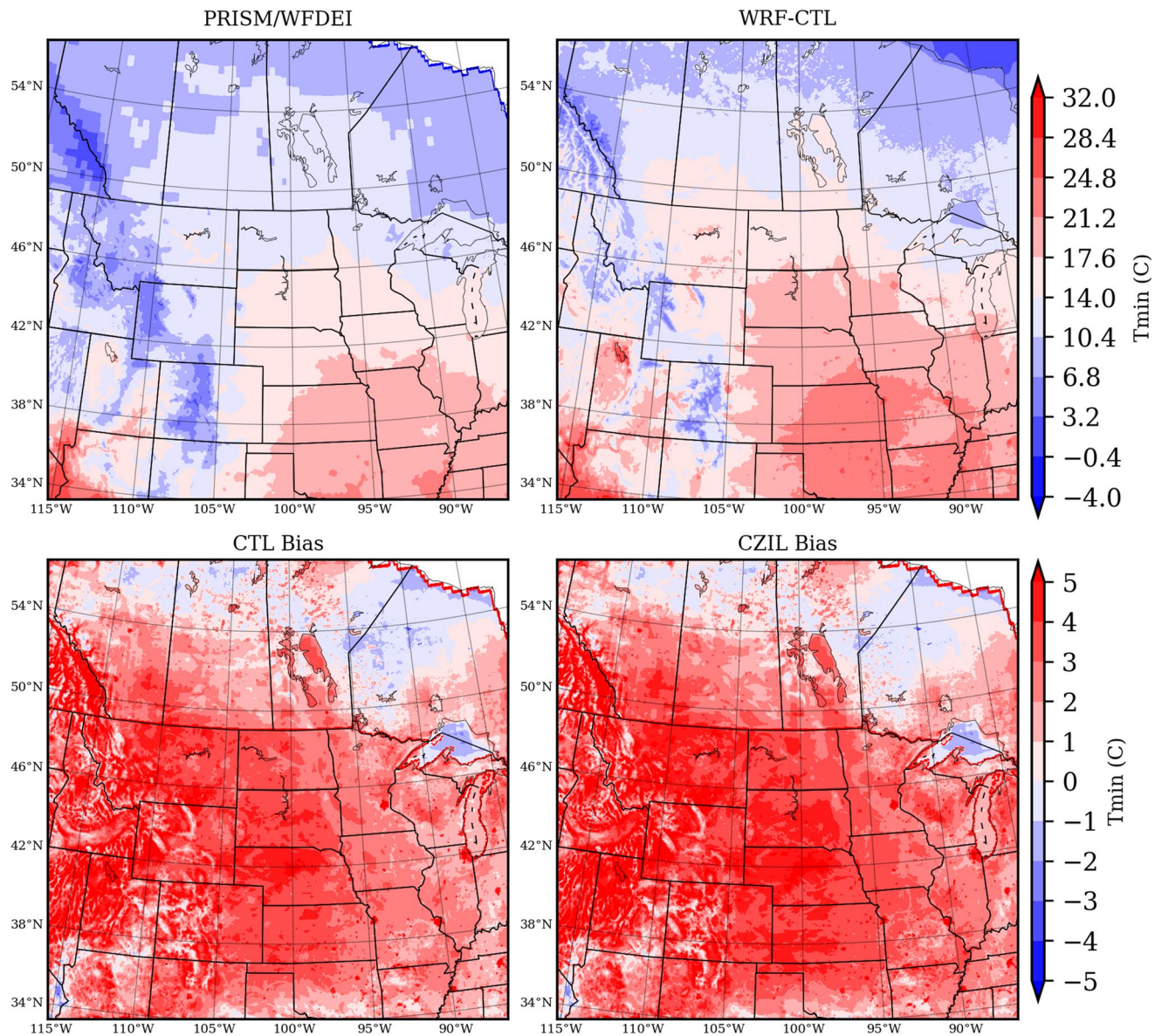


Fig. 14 Same as Fig. 13, except for summer (JJA)

2017). There are other issues related to the warm bias, such as little cloud cover resulting in more solar radiation, less precipitation, and soil moisture with less evaporative cooling. These could also lead to the consequences of warm bias, yet they are beyond the scope of this paper. Another interesting finding related to the new C_{zil} scheme is that the C_h and energy fluxes simulated over grassland in summer have less bias than in spring, especially in offline simulations. The seasonal change of canopy height is not represented in our configuration of Noah-MP. Instead the change in Z_{0m} is implemented through the seasonal change of the green vegetation fraction. Through Eq. (4), the seasonal change of the vegetation fraction can affect the ratio between Z_{0t} and Z_{0m} .

The other two schemes (the default $C_{zil} = 0$ and $C_{zil} = 0.1$) neglect the dependence of coupling strength on canopy height, which is bound to cause biases in coupling strength in grassland and forest. By decreasing C_h over grassland, the WRF-CZIL reduces the warm bias in T_{max} over the Great Plains and worsens the cold bias in T_{max} over the grassland near the Rockies.

Finally, although the updated simulations with the new $C_{zil}(h)$ scheme in the coupled WRF Noah-MP model improve the simulation of coupling strength in terms of the surface exchange coefficient in this study, many uncertainties and questions remain. These include uncertainties from inter-annual variability since it only covers two springs and

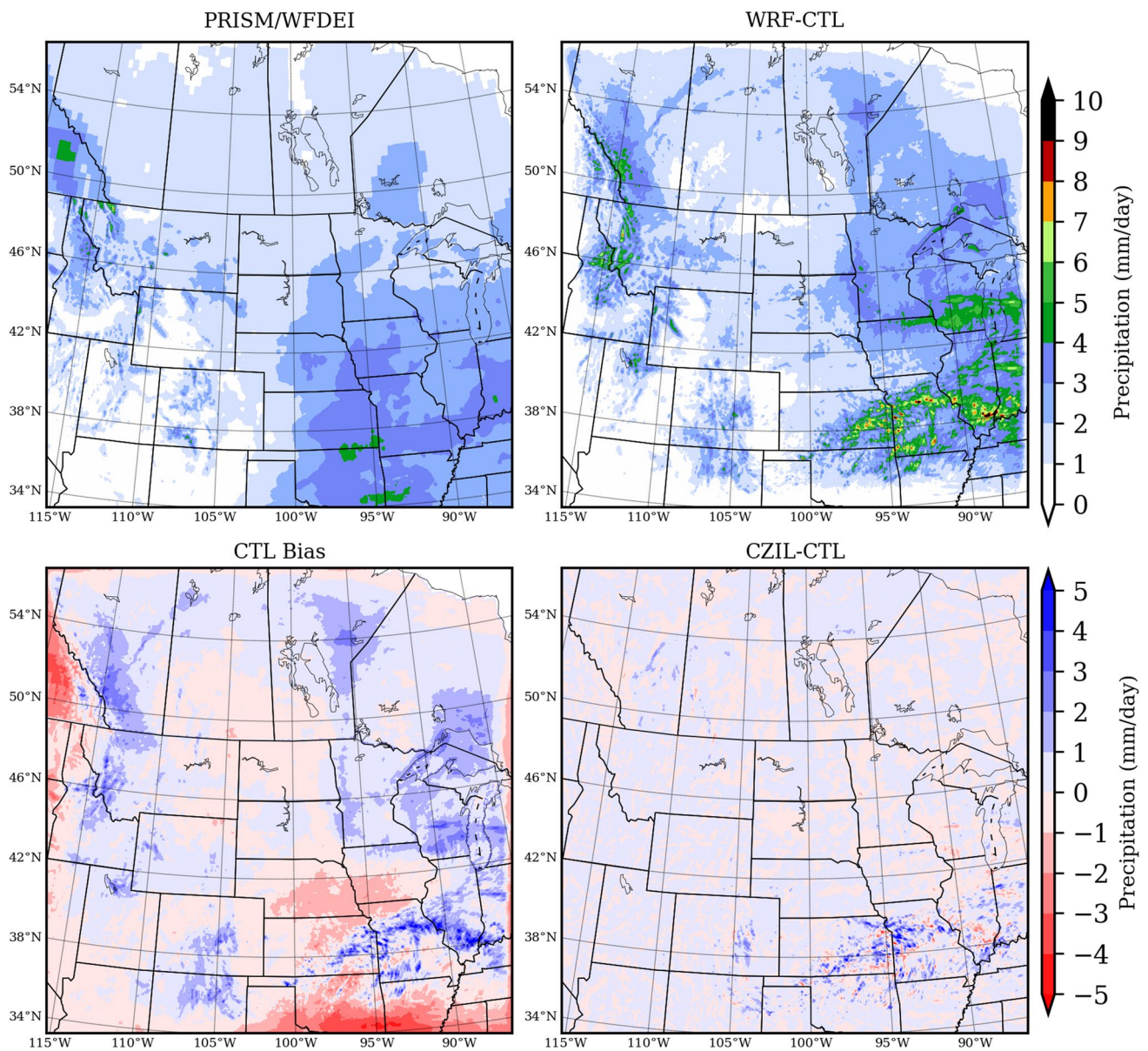


Fig. 15 Comparisons of precipitation from PRISM/WFDEI and coupled WRF model results in spring (MAM) of 2006, 2007. The top row shows the observation and WRF-CTL in mm/day. The bottom

row shows the WRF-CTL bias and the difference between WRF-CZIL and WRF-CTL in mm/day

summers, and the secondary and indirect effects induced by the new scheme through modifying surface heat flux, moisture flux, and flux partitioning. The difference in precipitation between the two C_{zil} schemes is not as clear as the difference in temperature because the impact of changing C_h is not local. WRF-CZIL improves the precipitation simulation compared to WRF-CTL by increasing the precipitation over cropland downwind of grassland and decreasing precipitation over forest where WRF-CTL overestimates it. The fully coupled effects of the new C_{zil} on precipitation and the water cycle need to be verified through an analysis of the

moisture flux/budget and precipitation events. Further studies with longer-term simulation using the new C_{zil} scheme implemented in the LSM and coupled with convection-permitting WRF are planned to resolve these uncertainties. Nevertheless, this study shows the potential for improving temperature simulation by correctly representing the surface exchange coefficient, especially through better simulation of sensible heat flux. These results will benefit hydrologists and atmospheric scientists who are interested in the response of the land surface to the atmosphere and climate systems in future modelling studies.

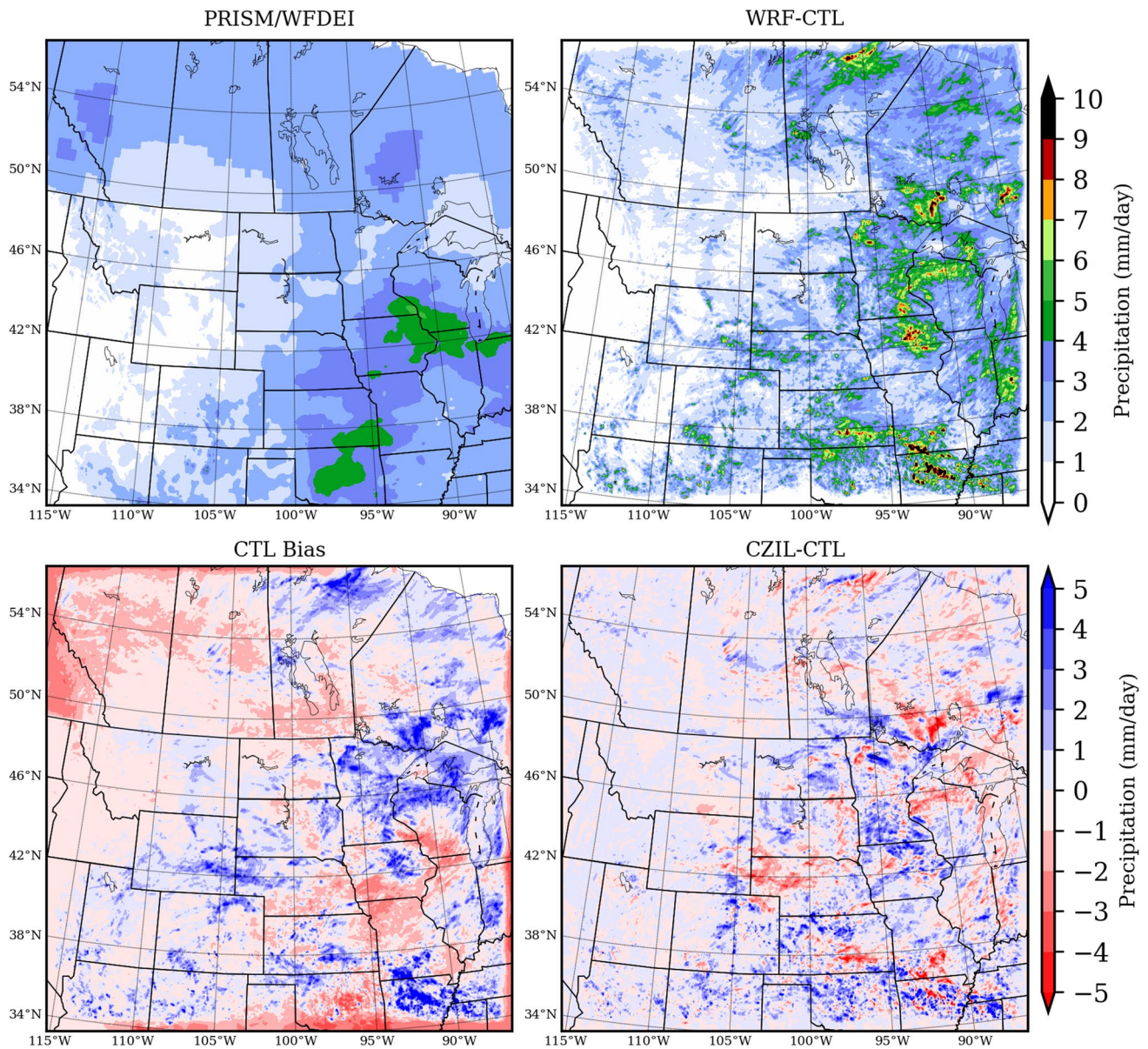


Fig. 16 Same as Fig. 15, except for summer (JJA)

Acknowledgements The authors Liang Chen gratefully acknowledges the support from the National Key Research and Development Program of China (grant number 2017YFC1501804) and the National Natural Science Foundation of China (grant number: 41875116). The authors Liang Chen, Yanping Li, Zhenhua Li and Zhe Zhang gratefully acknowledge the support from the Changing Cold Region Network (CCRN), Global Water Future (GWF) project and Global Institute of Water Security (GIWS) at University of Saskatchewan. Fei Chen, Michael Barlage appreciate the support from the Water System Program at the National Center for Atmospheric Research (NCAR), USDA NIFA Grants 2015-67003-23508 and 2015-67003-23460, and NSF Grant #1739705. NCAR is sponsored by the National Science Foundation. Any opinions, findings, conclusions or recommendations expressed in this publication are those of the authors and do not necessarily reflect the views of the National Science Foundation.

References

- Barlage M, Tewari M, Chen F, Miguez-Macho G, Yang ZL, Niu GY (2015) The effect of groundwater interaction in North American regional climate simulations with WRF/Noah-MP. *Clim Change* 129(3–4):485–498. <https://doi.org/10.1007/s10584-014-1308-8>
- Brutsaert W (1982) *Evaporation into the atmosphere*. Springer Netherlands, Dordrecht
- Chang HI, Kumar A, Niyogi D, Mohanty UC, Chen F, Dudhia J (2009) The role of land surface processes on the mesoscale simulation of the July 26, 2005 heavy rain event over Mumbai, India. *Global Planet Change* 67(1–2):87–103. <https://doi.org/10.1016/j.gloplacha.2008.12.005>
- Chen F, Dudhia J (2001) Coupling an advanced land surface-hydrology model with the Penn State-NCAR MM5 modeling system. Part I: Model implementation and sensitivity. *Mon*

- Weather Rev 129(4):569–585. [https://doi.org/10.1175/1520-0493\(2001\)129%3c0569:Caalsh%3e2.0.Co;2](https://doi.org/10.1175/1520-0493(2001)129%3c0569:Caalsh%3e2.0.Co;2)
- Chen F, Zhang Y (2009) On the coupling strength between the land surface and the atmosphere: from viewpoint of surface exchange coefficients. *Geophys Res Lett.* <https://doi.org/10.1029/2009gl0137980>
- Chen F, Mitchell K, Schaake J, Xue YK, Pan HL, Koren V, Duan QY, Ek M, Betts A (1996) Modeling of land surface evaporation by four schemes and comparison with FIFE observations. *J Geophys Res Atmos* 101(D3):7251–7268. <https://doi.org/10.1029/95jd02165>
- Chen F, Janjic Z, Mitchell K (1997) Impact of atmospheric surface-layer parameterizations in the new land-surface scheme of the NCEP mesoscale Eta model. *Bound Layer Meteorol* 85(3):391–421. <https://doi.org/10.1023/A:1000531001463>
- Chen L, Li Y, Chen F, Barr A, Barlage M, Wan B (2016) The incorporation of an organic soil layer in the noah-mp land surface model and its evaluation over a boreal aspen forest. *Atmos Chem Phys* 16(13):8375–8387. <https://doi.org/10.5194/acp-16-8375-2016>
- Decker M, Pitman A, Evans J (2015) Diagnosing the seasonal land-atmosphere correspondence over northern australia: dependence on soil moisture state and correspondence strength definition. *Hydrol Earth Syst Sci* 19(8):3433–3447. <https://doi.org/10.5194/hess-19-3433-2015>
- Dickinson RE (2011) Coupled atmospheric circulation models to biophysical, biochemical, and biological processes at the land surface. In: Donner L, Schubert W, Somerville R (eds) *The development of atmospheric general circulation models*, Cambridge University Press, 255+ xvipp
- Dee DP, Uppala SM, Simmons AJ, Berrisford P, Poli P, Kobayashi S, Andrae U, Balmaseda MA, Balsamo G, Bauer P, Bechtold P, Beljaars ACM, van de Berg L, Bidlot J, Bormann N, Delsol C, Dragani R, Fuentes M, Geer AJ, Haimberger L, Healy SB, Hersbach H, Hólm EV, Isaksen I, Kållberg P, Köhler M, Matricardi M, McNally AP, Monge-Sanz BM, Morcrette J-J, Park B-K, Peubey C, de Rosnay P, Tavolato C, Thépaut J-N, Vitart F (2011) The ERA-interim reanalysis: configuration and performance of the data assimilation system. *Q J R Meteorol Soc* 137(656):553–597
- Dirmeyer PA (2000) Using a global soil wetness dataset to improve seasonal climate simulation. *J Clim* 13(16):2900–2922. [https://doi.org/10.1175/1520-0442\(2000\)013%3c2900:Uagswd%3e2.0.Co;2](https://doi.org/10.1175/1520-0442(2000)013%3c2900:Uagswd%3e2.0.Co;2)
- Dirmeyer PA (2011) The terrestrial segment of soil moisture-climate coupling. *Geophys Res Lett.* <https://doi.org/10.1029/2011GL048268>
- Fischer EM, Seneviratne SI, Vidale PL, Luthi D, Schar C (2007) Soil moisture—atmosphere interactions during the 2003 European summer heat wave. *J Clim* 20(20):5081–5099. <https://doi.org/10.1175/Jcli4288.1>
- Garrat JR (1992) *The atmospheric boundary layer*. Cambridge University Press, New York
- Guo ZC, Dirmeyer PA (2013) Interannual variability of land-atmosphere coupling strength. *J Hydrometeorol* 14(5):1636–1646. <https://doi.org/10.1175/Jhm-D-12-0171.1>
- Guo ZC et al (2006) GLACE: the global land-atmosphere coupling experiment. Part II: analysis. *J Hydrometeorol* 7(4):611–625. <https://doi.org/10.1175/Jhm511.1>
- Hirsch AL, Pitman AJ, Kala J (2014) The role of land cover change in modulating the soil moisture-temperature land-atmosphere coupling strength over Australia. *Geophys Res Lett* 41(16):5883–5890. <https://doi.org/10.1002/2014gl061179>
- Kang SL, Davis KJ, LeMone M (2007) Observations of the ABL structures over a heterogeneous land surface during IHOP_2002. *J Hydrometeorol* 8(2):221–244. <https://doi.org/10.1175/Jhm567.1>
- Knist S et al (2017) Land-atmosphere coupling in EURO-CORDEX evaluation experiments. *J Geophys Res Atmos* 122(1):79–103. <https://doi.org/10.1002/2016jd025476>
- Koster RD, Dirmeyer PA, Hahmann AN, Ijpeelaar R, Tyahla L, Cox P, Suarez MJ (2002) Comparing the degree of land-atmosphere interaction in four atmospheric general circulation models. *J Hydrometeorol* 3:363–375
- Koster RD, Suarez MJ, Higgins RW, Van den Dool HM (2003) Observational evidence that soil moisture variations affect precipitation. *Geophys Res Lett.* <https://doi.org/10.1029/2002gl016571>
- Koster RD et al (2004) Regions of strong coupling between soil moisture and precipitation. *Science* 305(5687):1138–1140. <https://doi.org/10.1126/science.1100217>
- Koster RD et al (2006) GLACE: the global land-atmosphere coupling experiment. Part I: overview. *J Hydrometeorol* 7(4):590–610. <https://doi.org/10.1175/Jhm510.1>
- Kumar P, Kishtawal CM, Pal PK (2014) Impact of satellite rainfall assimilation on weather research and forecasting model predictions over the indian region. *J Geophys Res Atmos* 119(5):2017–2031. <https://doi.org/10.1002/2013jd020005>
- LeMone MA, Tewari M, Chen F, Alfieri JG, Niyogi D (2008) Evaluation of the Noah land surface model using data from a fair-weather IHOP_2002 day with heterogeneous surface fluxes. *Mon Weather Rev* 136(12):4915–4941. <https://doi.org/10.1175/2008mwr2354.1>
- Liu CH, Ikeda K, Rasmussen R, Barlage M, Newman AJ, Prein AF, Chen F, Chen L, Clark M, Dai A, Dudhia J, Eidhammer T, Gochis D, Gutmann E, Kurkute S, Li Y, Thompson G, Yates D (2017) Continental-scale convection-permitting modeling of the current and future climate of North America. *Clim Dyn* 49(1):71–95. <https://doi.org/10.1007/s00382-016-3327-9>
- Lorenz R, Pitman AJ, Hirsch AL, Srbinovsky J (2015) Intraseasonal versus interannual measures of land-atmosphere coupling strength in a global climate model: glace-1 versus glace-cmp5 experiments in access1.3b. *J Hydrometeorol* 16(5):2276–2295. <https://doi.org/10.1175/jhm-d-14-0206.1>
- Miralles DG, Berg MJ, Teuling AJ, Jeu RAM (2012) Soil moisture-temperature coupling: a multiscale observational analysis. *Geophys Res Lett.* <https://doi.org/10.1029/2012gl053703>
- Musselman KN, Clark MP, Liu C, Ikeda K, Rasmussen R (2017) Slower snowmelt in a warmer world. *Nat Clim Change* 7(February):214–220. <https://doi.org/10.1038/NCLIMATE3225>
- Musselman KN, Lehner F, Ikeda K, Clark MP, Prein AF, Liu C et al (2018) Projected increases and shifts in rain-on-snow flood risk over western North America. *Nat Clim Change* 8(9):808–812. <https://doi.org/10.1038/s41558-018-0236-4>
- Niu GY, Yang ZL, Mitchell KE, Chen F, Ek MB, Barlage M et al (2011) The community. Noah land surface model with multiparameterization options (Noah-MP): I model description and evaluation with local-scale measurements. *J Geophys Res Atmos* 116(12):1–19. <https://doi.org/10.1029/2010JD015139>
- Niyogi DS, Raman S, Alapaty K (1999) Uncertainty in the specification of surface characteristics, part II: hierarchy of interaction-explicit statistical analysis. *Bound Layer Meteorol* 91(3):341–366. <https://doi.org/10.1023/A:1002023724201>
- Overgaard J, Rosbjerg D, Butts MB (2006) Land-surface modelling in hydrological perspective—a review. *Biogeosciences* 3(2):229–241
- Pielke RA (2001) Influence of the spatial distribution of vegetation and soils on the prediction of cumulus convective rainfall. *Rev Geophys* 39(2):151–177. <https://doi.org/10.1029/1999rg000072>
- Prein AF, Rasmussen RM, Ikeda K, Liu C, Clark MP, Holland GJ (2016) The future intensification of hourly precipitation extremes. *Nat Clim Change* 7(1):48–52. <https://doi.org/10.1038/nclimate3168>
- PRISM Climate Group (2004) Oregon State University PRISM dataset. Oregon State University, Corvallis, Oregon. <http://prism.oregonstate.edu>. Accessed 4 Feb 2014
- Raghavendra A, Dai A, Milrad SM, Cloutier-Bisbee SR (2019) Floridian heatwaves and extreme precipitation: future

- climate projections. *Clim Dyn* 52(1–2):495–508. <https://doi.org/10.1007/s00382-018-4148-9>
- Rasmussen R, Liu C (2017) High resolution WRF simulations of the current and future climate of North America. Research Data Archive at the National Center for Atmospheric Research, Computational and Information Systems Laboratory, Boulder. <https://doi.org/10.5065/D6V40SXP>
- Rasmussen R et al (2011) High-resolution coupled climate runoff simulations of seasonal snowfall over Colorado: a process study of current and warmer climate. *J Clim* 24(12):3015–3048. <https://doi.org/10.1175/2010jcli3985.1>
- Rasmussen KL, Prein AF, Rasmussen RM, Ikeda K, Liu C (2017) Changes in the convective population and thermodynamic environments in convection-permitting regional climate simulations over the United States. *Clim Dyn* 0123456789:1–26. <https://doi.org/10.1007/s00382-017-4000-7>
- Salamanca F, Zhang Y, Barlage M, Chen F, Mahalov A, Miao S (2018) Evaluation of the WRF-urban modeling system coupled to Noah and Noah-MP land surface models over a semiarid urban environment. *J Geophys Res Atmos* 123(5):2387–2408
- Santanello JA, Peters-Lidard CD, Kumar SV, Alonge C, Tao WK (2009) A modeling and observational framework for diagnosing local land-atmosphere coupling on diurnal time scales. *J Hydrometeorol* 10(3):577–599. <https://doi.org/10.1175/2009jhm1066.1>
- Scaff L, Prein AF, Li Y, Liu C, Rasmussen R, Ikeda K (2019) Simulating the convective precipitation diurnal cycle in North America's current and future climate. *Clim Dyn*. <https://doi.org/10.1007/s00382-019-04754-9>
- Sellers PJ, Dickinson RE, Randall DA, Betts AK, Hall FG, Berry JA, Collatz GJ, Denning AS, Mooney HA, Nobre CA, Sato N, Field CB, Henderson-Sellers A (1997) Modeling the exchanges of energy, water, and carbon between continents and the atmosphere. *Science* 275:502–509. <https://doi.org/10.1126/science.275.5299.502>
- Seneviratne SI, Luthi D, Litschi M, Schar C (2006) Land-atmosphere coupling and climate change in Europe. *Nature* 443(7108):205–209. <https://doi.org/10.1038/nature05095>
- Seneviratne SI, Corti T, Davin EL, Hirschi M, Jaeger EB, Lehner I, Orlowsky B, Teuling AJ et al (2010) Investigating soil moisture-climate interactions in a changing climate: a review. *Earth Sci Rev* 99(3–4):125–161. <https://doi.org/10.1016/j.earscirev.2010.02.004>
- Stull RB (ed) (1988) An introduction to boundary layer meteorology. Springer Netherlands, Dordrecht
- Sun J (1999) Diurnal variations of thermal roughness height over a grassland. *Bound Layer Meteorol* 92(3):407–427
- Sun J, Mahrt L (1995) Determination of surface fluxes from the surface radiative temperature. *J Atmos Sci* 52:1096–1106. [https://doi.org/10.1175/1520-0469\(1995\)052<1096:DOSFFT>2.0.CO;2](https://doi.org/10.1175/1520-0469(1995)052<1096:DOSFFT>2.0.CO;2)
- Trier SB, Chen F, Manning KW (2004) A study of convection initiation in a mesoscale model using high-resolution land surface initial conditions. *Mon Weather Rev* 132(12):2954–2976. <https://doi.org/10.1175/Mwr2839.1>
- Trier SB, Chen F, Manning KW, LeMone MA, Davis CA (2008) Sensitivity of the PBL and precipitation in 12-day simulations of warm-season convection using different land surface models and soil wetness conditions. *Mon Weather Rev* 136(7):2321–2343. <https://doi.org/10.1175/2007mwr2289.1>
- Wan B, Gao Z, Chen F, Lu C (2017) Impact of tibetan plateau surface heating on persistent extreme precipitation events in southeastern China. *Mon Weather Rev* 145(9):3485–3505
- Weedon GP, Balsamo G, Bellouin N, Gomes S, Best MJ, Viterbo P (2014) The WFDEI meteorological forcing data set: WATCH Forcing data methodology applied to ERA-Interim reanalysis data. *Water Resour Res*. <https://doi.org/10.1002/2014wr015638>
- Xu X, Chen F, Shen S, Miao S, Barlage M, Guo W, Mahalov A (2018) Using WRF-urban to assess summertime air conditioning electric loads and their impacts on urban weather in Beijing. *J Geophys Res Atmos* 123(5):2475–2490
- Yang ZL, Niu GY, Mitchell KE, Chen F, Ek MB, Barlage M et al (2011) The community Noah land surface model with multiparameterization options (Noah-MP): 2. Evaluation over global river basins. *J Geophys Res Atmos*. <https://doi.org/10.1029/2010JD015140>
- Zhang Z, Li Y, Chen F, Barlage M, Li Z (2018) Evaluation of convection-permitting WRF CONUS simulation on the relationship between soil moisture and heatwaves. *Clim Dyn*. <https://doi.org/10.1007/s00382-018-4508-5>
- Zheng Y, Kumar A, Niyogi D (2015) Impacts of land-atmosphere coupling on regional rainfall and convection. *Clim Dyn* 44(9–10):2383–2409
- Zilitinkevich S (1970) Non-local turbulent transport: pollution dispersion aspects of coherent structure of convective flows. *Air Pollution III*, vol 1: air pollution theory and simulation, pp 53–60

Publisher's Note Springer Nature remains neutral with regard to jurisdictional claims in published maps and institutional affiliations.